ChemistrySelect

ChemistrySelect
Chemistry Europe
European Chemical Societies Publishing

RESEARCH ARTICLE

Graphene-Stabilized Borophane Composite Anode for High Performance Lithium-ion (Li-ion) Batteries

Nallathambi Suman[1] | Thirunavukkarasu Somanathan[1] | Andikkadu Masilamani Shanmugharaj[2] | Jayaraman Balamurugan[3]

[1]Department of Chemistry, Vels Institute of Science, Technology and Advanced Studies (VISTAS), Chennai, India | [2]Department of Chemistry, Sri Sivasubramaniya Nadar College of Engineering (SSNCE), Chennai, India | [3]Department of Materials Science & Engineering, Korea Advanced Institute of Science and Technology (KAIST), Daejeon, Republic of Korea

Correspondence: Thirunavukkarasu Somanathan (soma.sbs@vistas.ac.in)

Received: 3 October 2025 | **Revised:** 11 February 2026 | **Accepted:** 18 February 2026

Keywords: anode materials | borophane | graphene | hydroboration | LiB

ABSTRACT

The outstanding mechanical and electronic properties of borophane make it an ideal candidate for nanoelectronics applications, In addition, higher Li loading amount ($Li_{0.445}B_2H_2$) with theoretical capacity as high as 504 mAh/g consistent to the theoretical binding energy analysis of lithium atoms on borophane, makes it point of angle to focus promising anode aspirant for lithium-ion batteries. Though, volume expansion is quite inevitable in these types of materials, thus hampering its application aspect in Li-ion battery anodes. Also, as far as we know, no actual testing investigation was made in exploring it as an anode for energy storage applications. In the present study, novel borophane-graphene composite has been synthesized by controlling the chemical properties at the boundary between the two materials borophane and oxygenated derivative of graphene (i.e.) graphene oxide and subsequently used it as an anode material for Li-ion batteries. The main reason for this study of making composite is to combine the complementary advantages of both materials while overcoming their individual limitations, especially for energy storage (Li-ion battery anode) applications. Synthesis of borophane-graphene composite involves two steps with the first step being the synthesis of borophane from magnesium boride followed by the hydroboration reaction on graphene oxide sheets generating borophane-graphene composites. Successful synthesis of borophane-graphene composites has been corroborated using various characterization tools Electrochemical characterization of lithium ion half cells fabricated using borophane-graphene composite anode delivers the amount of electric charge during discharge of 627 $mAhg^{-1}$, with the reversible discharge ability of 404 $mAhg^{-1}$ after test involving repeated 100 cycles, ensuring it as a perspective anode option for lithium-ion (Li-ion) battery technology.

1 | Introduction

Owing to the high specific surface area, quasi-2D electron confinement, flexibility and distinctive material properties, two-dimensional (2D) nanostructures containing of one or a small number of layered atomic arrangements exhibit outstanding performance in a variety of applications, when compared to their bulk counterparts [1, 2]. Interestingly, controlled stacking of 2D layered materials results in the development of emerging three dimensional (3D) van der Waals heterostructure with layered architecture provides unusual properties and functionalities [3]. In contrast to the bulk materials, van der Waals heterostructures prepared through the precise assembly of 2D materials is effective in engineering optoelectronic behaviour that could not be attained under normal circumstances. The concept of designing van der Waals heterostructures through deliberate layering of different 2D materials become thought provocative as they can lead to novel 3D materials with exciting

physical phenomena due to the synergistic contribution of the individual 2D materials [4]. For instance, controlled stacking of hexagonal boron nitride (HBN) and graphene nanostructures resulted in the development of transistors with outstanding density independent electron mobility ($\mu_c \approx 60\,000\ cm^2\ V^{-1}\ s^{-1}$) [4, 5]. The field effect tunnelling transistors (FETT) fabricated using stacked layers of graphene and various 2D materials (such as boron nitride, molybdenum sulfide and tungsten disulfide) enables quantum electron tunnelling with improved on/off ratio, thus making it as the potential transistors. In addition, the optoelectronic properties, photo-responsive memory and non-volatile memory functionalities can effectively be manipulated in these stacked layers due to the shorter transfer length [6]. Development of 3D nanostructured material with controlled stacking of 2D graphene and inorganic 2D materials has also significant impact on the energy storage applications. For instance, heterostructures based on 2D graphene and siloxane nanosheets resulted in the development of high performance anode material for lithium-ion (Li-ion) batteries rendering long term electrochemical cycling behavior with reversible specific capacity as high as 1040 $mAhg^{-1}$ after 1000 cycles [7]. Similarly, controlled stacking of graphene-molybdenum disulfide (G-MoS_2) nanostructures resulted in the development of a composite paper that can potentially store sodium-ions (Na-ions) and also behave as the flexible current collector, when functioning as an electrode in sodium-ion batteries. According to their report, the fabricated composite paper electrode delivers stable charge capacity of 230 $mAhg^{-1}$, with respect to the weight of the total electrode [8]. Likewise, heterostructured composite electrode based on reduced graphene oxide (RGO) and titanium carbide ($Ti_3C_2T_x$) nanomaterials exhibit a specific capacitance as high as 140 Fg^{-1} thus making it as a potential candidate for the fabrication of robust, high performance stretchable supercapacitor [9]. For the development of novel heterostructure with outstanding electrochemical performance, in both lithium-ion (Li-ion) and sodium-ion (Na-ion) batteries [10, 11] the controlled stacking of 2D phosphorene and graphene being employed as an anode material.

Owing to its inherent metallic conductivity, single layer boron sheets, termed as borophene, has risen as a new exciting 2D material possessing unique electronic, mechanical and optical properties [12, 13]. Theoretical predictions revealed that the borophene serving as ideal anode material with outstanding electrochemical characteristics for both of Li and Na-ion batteries [14]. However, the preparation methods of borophene nanosheets reported so far is the bottom-up (Upward) approach, which incorporate chemical vapour deposition [15] and molecular beam epitaxy on metallic surfaces [16–18]. On the otherhand, hydrogenated derivatives of borophene sheets (termed as borophane) have received wide attention among researchers due to its excellent hydrogen storage capacity in addition to the unique electronic and mechanical properties [19]. Nishino et al., [20] first reported the experimental method of preparing borophane nanosheets with an empirical formula H_1B_1 via., cation exchange reaction of magnesium diboride (MgB_2). Density functional theory (DFT) studies of the borophane nanosheets revealed that the theoretical lithium storage capacity (~504 mAh/g) may appear moderate, its ultralow mass density, high specific surface area, and fast Li-ion diffusion pathways [21, 22] make it a promising 2D anode candidate. However, its major drawbacks—namely chemical instability, layer stacking, and poor conductivity reduce the practical capacity (<100 $mAh\ g^{-1}$) [23].

In the present research, a novel borophane-graphene based composite anode have been prepared to address the key issue faced by the borophane nanosheet based anodes. This composite improves the electrical conductivity because graphene forms a continuous conductive network, it facilitate rapid electron transport from borophane active sites also reduces the charge-transfer resistance. Moreover this composite enhance the structural stabilization, as graphene behaves as a mechanical buffer to prevent borophane restacking, collapsing the structure during lithiation, and improves cycling stability. This composite provides suppression of volume expansion, increase ion diffusion and active sites and last the chemical stability, Hydrogen-passivated borophane is more stable than borophene and further the addition graphene shields the borophane from oxidation and improve the environment durability. The prepared composites were characterized using various tools to corroborate structural, morphological and chemical characteristics. 2032 type coin cells were fabricated with lithium metal using the prepared borophane-graphene composites as anode, also as counter and reference electrode and evaluated for its electrochemical properties. Incorporation of graphene layers between the borophane nanosheets effectively control its stacking behaviour, so when it is being used as an anode for lithium batteries, its improving the electrochemical performance characteristics.

2 | Experimental Section

2.1 | Synthesis of Borophane (BP) Nanosheets From MgB_2

To Synthesis the Borophane nanosheets (HBNs) the procedure was followed which reported by Nishano et al., [20]. In the typical experiment, desired quantity of MgB_2 powder was added to 100 mL acetonitrile containing 1 g of sulfonic acid containing ion-exchange resin. The reaction mixture was stirred in nitrogen environment under ambient conditions for three days. By doing the filtration the black precipitate obtained during the course of reaction was removed. The yellow-coloured filtrate was dried at 70°C in nitrogen environment to obtained yellow powder (HBNs) on the hot plate. Included in Figure 1 (a) is the visual explanation of the steps followed during the preparation of borophane (BP) nanosheets from MgB_2.

2.1.1 | Background

MgB_2 is the most widely used solid precursor because it already contains layered boron sheets separated by Mg^{2+} ions. The synthesis relies on topochemical ion-exchange.

MgB_2 crystal structure: Alternating layers of Mg^{2+} and hexagonal boron sheets

During synthesis: Mg atoms are removed, Hydrogen atoms bind to boron.

Boron layers are preserved → converted to B–H (borophane).

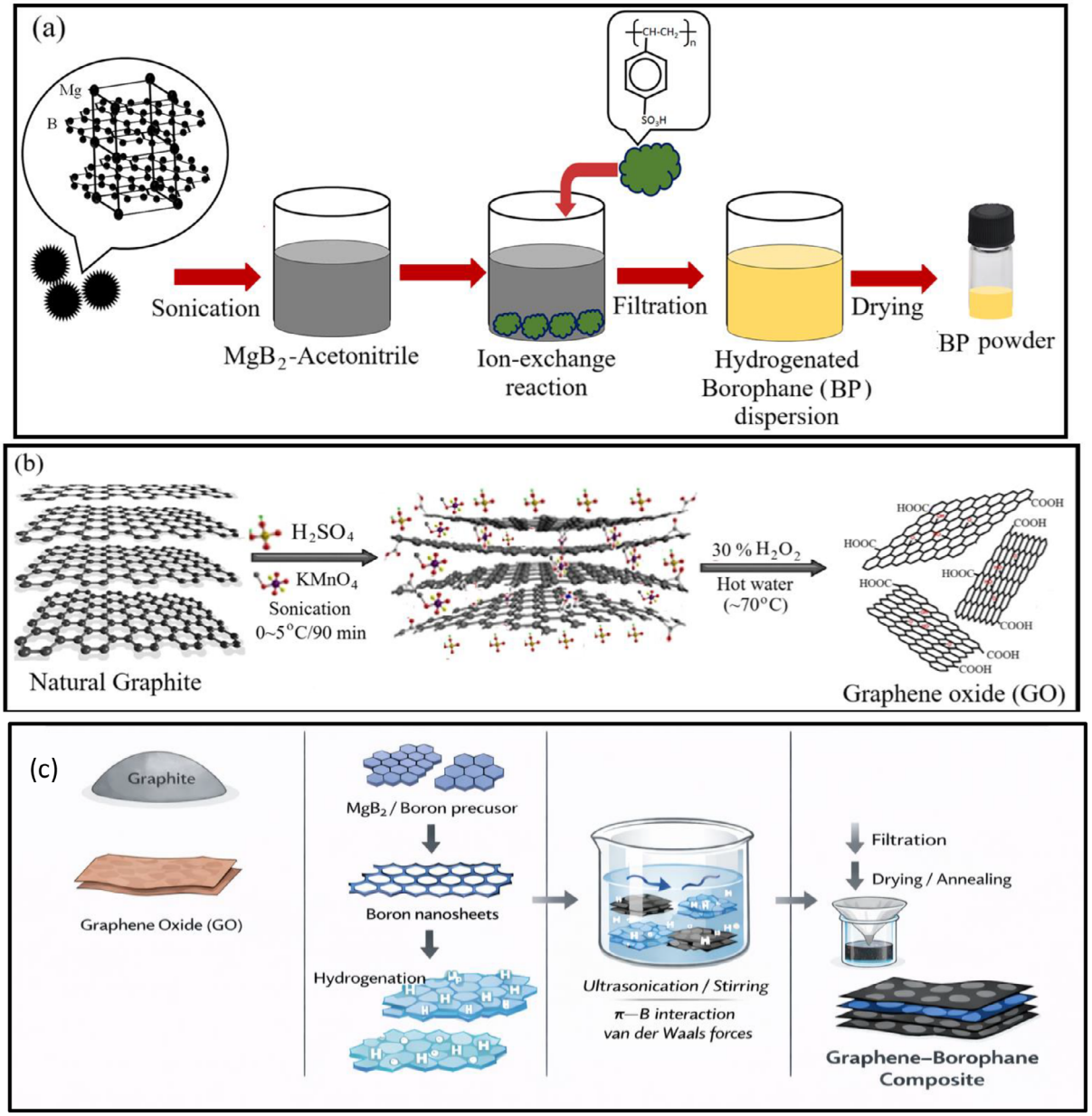

FIGURE 1 | Schematic representation on the preparation steps of (a) borophane powder (HBNs) powder from magnesium boride (MgB_2), (b) graphene oxide from natural graphite and (c) graphene-borophane composites.

2.2 | Stability of Borophene & Borophane

Borophene is unstable because, it is pure boron sheets, boron is electron-deficient, borophene has lot of dangling bonds, very high surface energy and extremely reactive with O_2 and H_2O which results rapid oxidation in air, structural distortion or collapse. But Borophane is relatively stable than Borophene, The key factor is hydrogen termination in Borophane, as hydrogen forms B–H covalent bonds, these bonds Saturate dangling bonds which reduce surface reactivity and suppress rapid oxidation and moisture attack this results in Free-standing sheets possible, also it improves significantly air and electrochemical stability and maintains 2D structure.

The boron lattice remains intact (topochemical stability), this makes borophane thermodynamically and kinetically stable than borophene.

Over the year time, the hydrogen desorption may occur due to heat, exposure to UV and vacuum annealing. Borophane stability may causes by Hydrogen desorption which creates reactive boron sites, Edge oxidation that starts at sheet boundaries, Defect-assisted oxidation due to that, Vacancies and wrinkles act as reaction centers. This happens gradually and not catastrophic. But the composite of Borophane with graphene protect the borophane and makes it chemically still stable.

2.3 | Safety Precautions

Chemical Hazards: MgB_2 can react with acids and moisture, releasing flammable hydrogen gas. should handle under dry conditions. Must avoid exposure to water unless explicitly intended and controlled.

Use of Acids / Etchants: Common Mg-removal processes involve strong acids which is corrosive to skin, eyes, and lungs can release toxic or flammable gases, always do under chemical fume hood, should wear acid-resistant gloves, lab coat, goggles, and face shield, add solids to liquids slowly (never the reverse). Ensures during the synthesis process no open flames, sparks, or hot surfaces nearby and ensuring good ventilation.

2.4 | Graphene Oxide Synthesis via Oxidation From Natural Graphite

The chemical exfoliation of natural graphite resulting in the formation of graphene oxide was done by adopting improved Hummer's method [23–25]. In concise, 5 grams of natural graphite was added with 250 mL of concentrated sulfuric acid and done the sonication for 60 min using a sonicator (S450D, 500 W, 30% amplitude) after that the addition of the desired quantity of sodium nitrate ($NaNO_3$) (5 g) kept under ice bath. Desired quantity of potassium permanganate ($KMnO_4$) (30 g) was gradually added to this mixture performed in ice-cold conditions and subjected to stirring for 2 h. The temperature of the reaction mixture was slowly elevated and retained at 35°C placed in a water bath for additional 60 min. This step is further proceeded by the addition of 230 mL of hot water (~70°C) and subsequently the temperature was raised to 98°C. Finally, 400 mL of hot water (~70°C) was added, after that 100 mL of 30% (wt) hydrogen peroxide (H_2O_2) solution to abort the reaction [26]. The synthesized graphite oxide was dispersed in water and purified by dialysis to remove the residual salts and acids completely. To produce GO powder, the GO was dried throughout the night at 70°C under vacuum (40 mm Hg). The schematic representation depicting the GO synthesis through modified Hummer's method is shown in Figure 1 (b).

2.5 | Preparation of Borophane-Graphene (GB) Composites

Desired quantity of borophane (HBNs) and graphene oxide (GO) nanosheets in tetrahydrofuran (THF) solvent (1 mg/mL) were stirred at room temperature for 24 h and subsequently dried under vacuum to generate black coloured powder of borophane-graphene (GB) composites. Schematics depicting the preparation of the GB composites is shown in Figure 1 (c).

2.6 | Borophane-Graphene Composites Differed From Boron/Graphene Based Anode Materials

Borophane provides capacity and Graphene provides conductivity and mechanical support, hydrogenation stabilizes boron and reduced restacking of sheets. With respect to the electrical mechanism, Boron-based anode has strong Li–B interaction, slow kinetics, irreversible Li trapping and large initial capacity loss. Graphene-based anode has Li intercalation / adsorption, fast kinetics, limited active sites, excellent reversibility but low capacity.

Borophane–graphene composite has dual-storage mechanism. Li adsorption on borophane, fast electron transport through graphene, buffered volume change, suppressed Li trapping. With respect to Conductivity and charge transport, Boron-based anodes has limited electronic pathways, Graphene-based anodes has excellent conductivity but few Li sites. But in case of Borophane-Graphene Composite, Graphene forms a continuous conductive network, Borophane acts as high-capacity active material and reduced charge-transfer resistance. In Mechanical and Cycling stability features also getting better with the composite as buffered volume expansion, suppressed pulverization and cycle life is improved. Overall the capacity of Borophane, conductivity and stability of Graphene with chemical passivation of Hydrogen makes the Borophane-Graphene composites can lead better features than the individual Boron/Graphene anode materials.

2.7 | Characterization Studies

Fourier transform IR spectroscopic (FT-IR) studies of MgB_2, BP and GB samples was performed by using a Perkin Elmer FT-IR spectrometer instrument (Model: Spectrum one, USA) in diffuse reflectance mode set at the resolution of 0.4 cm^{-1} between the wave number range of 4000 to 400 cm^{-1}. Powder X-ray diffraction (XRD) analysis of MgB_2, BH, GO and GB samples in the 2θ span of 5–80° was performed using a Rigaku Smart Lab X ray diffracto meter (SmartLab, Japan) equipped with a Copper target (40 kV, 20 mA, Kα1 = 1.54Å). Structural examination was done in the scale of 3900~100 cm^{-1} using Raman spectroscopy (Alpha 300R, WITec GmBH, Germany). The surface morphology and elemental compositions of the MgB_2, BP and GB samples were done using Field Emission Scanning Electron Microscopy (FE-SEM) (Quattro-S, Thermo Fischer Scientific, FEI Company, USA) equipped with energy dispersive x-ray analyzer (EDX). Morphological features is further investigated using transmission electron microscope (TEM, JEOL JSM, Japan). Surface chemical characteristics and functional sites was further determined using Versaprobe III X-ray photoelectron spectroscopy (PHI5000, ULVAC-PHI Ltd., Japan).

Electrodes were fabricated using a slurry coating technique, comprising 80 wt. % active materials (MgB_2, BP and GB), 10 wt % super P (TIMCAL) used as a conductive enhancer, and 10 wt % poly (vinylidene difluoride) (PVDF) (Kureha—KF100) as a binding material, applied over Cu foil serving as the conductive substrate. The paste was prepared by blending the specified constitution with N-methyl pyrrolidone (NMP) solvent in a mortar for about 15 min, followed by coating on top of the copper foil and dried out in an oven for about 10 h at 120°C temperature. Electrodes with a diameter of approximately 10 mm were extracted from the dried samples following compression under a load of 7T. The punched-out electrode with lithium metal as counter and reference electrode were fabricated into a coin cell (2032type) utilizing an electrolyte-soaked 8 μm thick polypropylene separator. In the commercial 1 M lithium hexafluorophosphate (LiPF6) electrolyte,

composed of a equal part mole ratio of dimethyl carbonate (DMC) and ethylene carbonate (EC), 1 wt % of NCQD was incorporated than utilized in the fabrication of lithium metal batteries.

2.8 | Electrochemical Characterization

The electrochemical investigations of MgB2, BP, and GB were conducted by constructing 2032 type Li-ion cells. The negative electrodes (based on MgB2, BP, and GB materials) were fabricated using a slurry coating method with weight ratios of 80:10:10 for the acetylene black, poly (vinylidene difluoride) (PVDF) binder and the active functional material. By blending the mixture with N-methyl pyrrolidone (NMP) solvent for 15 min in a mortar, the slurry was prepared, after which it was applied onto Cu foil and dried out at 120°C for about 10 h in an oven. From the dried electrode, discs of approximately 1.0 cm in diameter were punched and following that fabricated into (2032 type) coin cells utilizing mixture of lithium hexafluoro phosphate electrolyte (1 M LiPF6 in a 1:1 v/v o f ethylene carbonate and dimethyl carbonate mixture) and the counter/reference electrode is lithium metal foil. The electrochemical characteristics like charge and discharge of the assembled coin cells were evaluated within a voltage scale of 0.01 to 2 V versus Li/Li+ using a Neware battery analyser which was tested for the electrochemical characterization.

3 | Results and Discussion

Borophane nanosheets is the two-dimensional (2D) layered structures of hydrogen boride sheets with dirac cone configuration similar to that of graphene materials. However, unlike graphene, borophane has distorted and asymmetric dirac cone structures with fermi velocity, one order higher magnitude than that of graphene materials [21]. The uniqueness of the borophane is its ultra-high Fermi velocity resulting high carrier mobility that surpasses its rivalry (i. e.) graphene. Also, in contrast to metallic borophene, which is metallic in nature, the hydrogen boride sheets are semiconducting in nature due to its unique dirac cone configuration.

2D Borophane nanosheets can be synthesized from the AlB_2 type layered crystal structure such as magnesium diboride (MgB_2) through various synthetic routes [20, 27]. In the present study, ion-exchange method reported by Nishano et al., [20] has been adopted in synthesizing borophane nanosheets using the ion-exchange resin. Shown in Figure 1 (a) is the schematics depicting the preparation steps of yellow coloured borophane nanosheets from magnesium diboride (MgB_2). In order to realize the full application potential of borophane as an energy storage material, it needs to be surface engineered either by introducing active functional sites or by stacking with stable 2D materials such as graphene. In the present work, hieratically structured composite anode based on borophane and graphene has been designed using borophane and oxidized derivative of natural graphite (i.e.) graphene oxide (GO). Modified Hummers method has been employed in preparing graphene oxide (GO) consisting of various oxygen functionalities such as carboxylic acid (-COOH), hydroxyl (-OH) and epoxide groups as discussed in the experimental section (Figure 1 (b)). Finally, borophane-graphene composites have been successfully synthesized by using dispersions of individual components (~1 mg/mL) as discussed in the experimental section (Figure 1 (c)). Various tools used to characterize the resultant grey coloured composite material for corroborate the structural, chemical and morphological features.

X ray diffraction (XRD), Raman and Fourier Transform IR Spectroscopic (FTIR) results of the MgB_2, Borophane (BP) and borophane-graphene (BG) composites are included in Figure 2. Pristine MgB_2 displayed diffraction peaks at 2θ values of 26°, 34°, 42°, 51°, 60.5°, 64°, 66°, 70.5° and at 77° corresponding to the crystal planes of (001), (100), (101), (002), (110), (102), (111), (200) and (201), respectively. In addition, small diffraction peaks at 37° and at 62° revealed the presence of trace amount of MgO in the pristine MgB_2. De-intercalation of the magnesium ion (Mg-ion) through ion-exchange process resulted drastic variation in the crystal planes suggesting the absence of long range order. Appearance a broad peak at the 2θ value of 5° corroborates the formation of flexible nanosheets consisting of weak crystal planes [21]. In the formation of graphene oxide (GO), the chemical exfoliation of graphite resulting a strong peak at the 2θ value of 11° equivalent to the (001) crystal plane of the functionalized 2D graphene sheets (Figure not shown). On the contrary, borophane-graphene sheets displayed broad peak at 2θ values of 5° (diffraction peak corresponding to BP), 25° (002 crystal plane of graphene) and 44° (101 crystal plane of borophane) confirming the successful formation of the borophane-graphene composites [28]. The results of structural characterization of the MgB_2, BP, GO and GB was done using Raman spectroscopic studies and included in Figure 2 (b). In pristine MgB_2 [29], a single broad peak at 590 cm^{-1} with large lorentzian line-width that corresponds to the E_{2g} in-plane B stretching mode is observed. The appearance of broad peak at ~2800 cm^{-1} during de-intercalation of Mg-ion from the MgB_2 corresponding to B-H stretching confirms the formation of hydrogen boride nanosheets. Raman spectroscopic characterization of graphene oxide (GO) showed two characteristic peaks at 1590 and at 1350 cm^{-1} that corresponds to the E_{2g} phonon mode vibration of the sp^2 carbon atoms (G band) and breathing mode k-point phonons of A_{1g} symmetry (D-band) [30]. Interestingly, the peak corresponding to G band shift to higher wavenumber (~ 1600 cm^{-1}) with no noticeable deviation in D-band peak position (~1355 cm^{-1}) corroborating enhancement in the crystalline characteristics of the graphene phases of the borophane-graphene (BG) composites. The interfacial interaction defect healing controlled by borophane wih graphene improves the crystalline characterization. Borophane with 2D crystalline sheet and ordered B-B framework, when this composites with graphene strong π-B orbital interaction and van der waals coupling will occur, here borophane acts as a 2D crystalline support. This support from borophane restricts the random wrinkling of graphene sheets. So the in-plane ordering is improved, reduces the lattice distortion.

Borophane sheets also act as a spacers to maintain the interlayer separation to prevent random stacking of graphene. The graphene defects may cause high D-band intensity in Raman but when it is the composite with Borophane the hydrogenated borophane provide the electron density stabilization and interfacial bonding passivates graphene defect sites which results the increased crystalline domain and reduced defect scattering. This Graphene-Borophane composite distributes stress uniformly and reduce local lattice strain, so the narrower Raman G peak occur. The

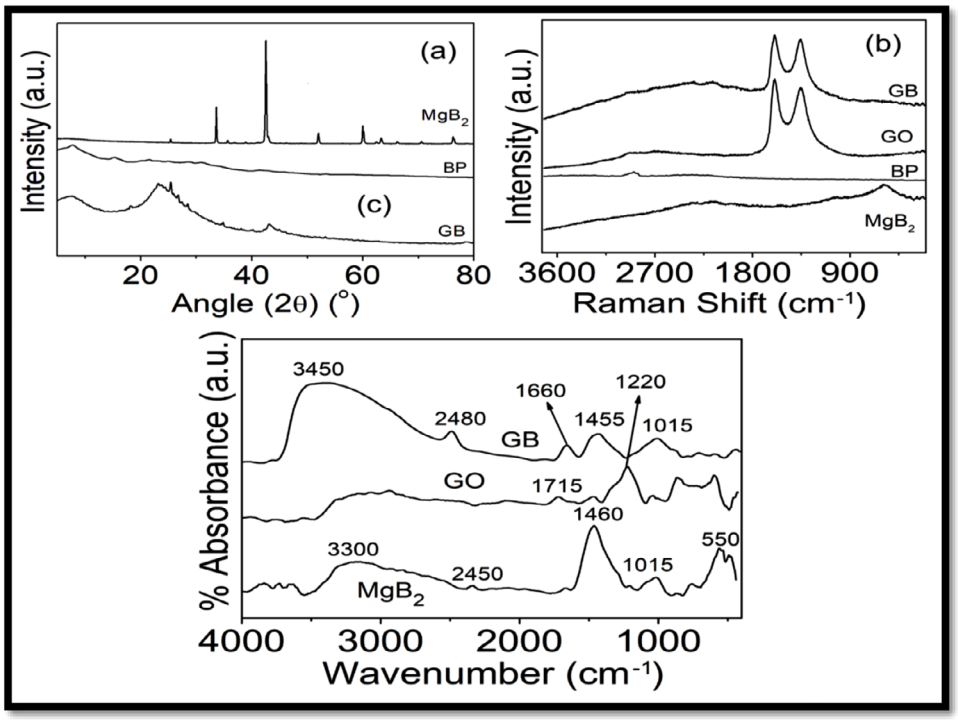

FIGURE 2 | (a) X-ray diffraction (b) Raman spectroscopic and (c) Fourier Transform Infrared Spectroscopic results of MgB_2, borophane (BP) and borophane-graphene (GB) composites.

upward shift of the G-band (~1600 cm^{-1}) in the composite arises from (i) Charge transfer interactions between borophane and graphene, which increase in-plane ordering, (ii) Strain-induced lattice modulation due to borophane incorporation, improving the crystalline domain size, (iii) Reduction of structural defects, as indicated by the stable D-band position. In comparison to graphene oxide (GO), slight shift in G band to higher wavenumber is due to the presence of P-type semiconductor (Borophane) in the GB anode.

The chemical characteristics of the MgB_2, GO and BG compounds are added in Figure 2 (c). The presence of various functionalities is confirmed in Pristine MgB_2, because it displayed four broad IR peaks at 3300, 2450, 1460, 1050 and at 550 cm^{-1} that are corresponds to –OH stretching in B-OH group, B-H stretching, B-O stretching, B-OH stretching and B-B stretching. Magnesium ion deintercalation by ion exchange method resulted in the appearance of two major peaks corresponding to B-H stretching and B-H-B stretching [20]. FTIR characterization displays the broad peaks corresponding to –OH stretching (~ 3400 cm^{-1}), 1715 cm^{-1} (>C = O stretching of -COOH group), 1220 cm^{-1} (-C-O stretching of epoxide group) and 550 cm^{-1} (Mg-B stretching) confirming the presence of oxygen functionalities on the GO surface. On the otherhand, borophane-graphene composites displayed several IR peaks which are corresponds to –OH stretching (~3400 cm^{-1}; OH groups in C-OH, -COOH etc.), B-H stretching (2480 cm^{-1}), >C = O stretching of –COOH group (1660 cm^{-1}), -CH bending vibrations (1455 cm^{-1}) and C-B stretching vibrations (1015 cm^{-1}) corroborating interfacial interactions between the graphene and borophane surfaces. The feasible mechanism of interface between the borophane and graphene is depicted in Figure 3. It is expected that borophane nanosheets, which has B-H functionalities on its surface reacts with functionalities of graphene oxide by possible reactions. The epoxide groups present in the GO surface undergoes ring opening reaction with B-H group to C-B and B-OH bonds. Alternatively, sp2 hybridized carbon near the broken edges of GO can undergo hydroboration reaction resulting in the formation C-B bonds as proposed in the scheme. The above facts are further supported by the XPS results (Figure 4). Survey scan results of MgB_2, BP and GB showed the peaks corresponds to Mg2s (90 eV), Mg2p (50 eV), B1s (~190 eV), MgKLL (300 eV) and O1s (~530 eV) peaks (Figure 4 (a)). In addition to this, borophane-graphene composites showed an strong peak at 285 eV correlated to C1s peak confirms the presence of graphene in the composites. High resolution spectral studies pertaining to the boron, oxygen and carbon has been done and the deconvoluted peaks are shown in Figure 4 (b-h). Data correction of B1s spectra of MgB_2 showed three characteristic peaks at 186.6 eV, 187.1 eV 192 eV that corresponds to MgB_2 (boron as boride anion), metallic boron, and boron trioxide (B_2O_3), respectively (Figure 4 (b)) [31]. As MgB_2 is vulnerable to oxidation, single peak at 531.7 eV is observed in the high resolution O1s spectra corroborating the presence of magnesium oxide (MgO) (Figure 4 (c)). High resolution B1s spectra of BP showed three peaks at 187.9 (B-H-B), 189.6 (B-H) and at 192.6 eV (B-OH) corroborating successful formation of 2D hydrogen boride nanosheets (Figure 4 (d)) [32]. The appearance of strong O1s peak at 532.3 eV (B-OH group) (Figure 4 (e) is the further evidence for the he presence of oxidized borophane nanosheets. Similarly, the borophane-graphene composites (BG) showed three broad peaks at 187.7 (B-H-B), 188.7 (C-B) and 192.6 (B-OH). The appearance of strong peak at 188.7 eV corroborates the formation boron-carbon linkages as proposed in the schematic representation (Figure 3) [33]. The deconvoluted C1s spectra is the further evidence for the interfacial interaction between the borophane and graphene nanosheets, because it has showed four major peaks at 283.9 (C-B), 284.7 (C-C/C-H), 286.5

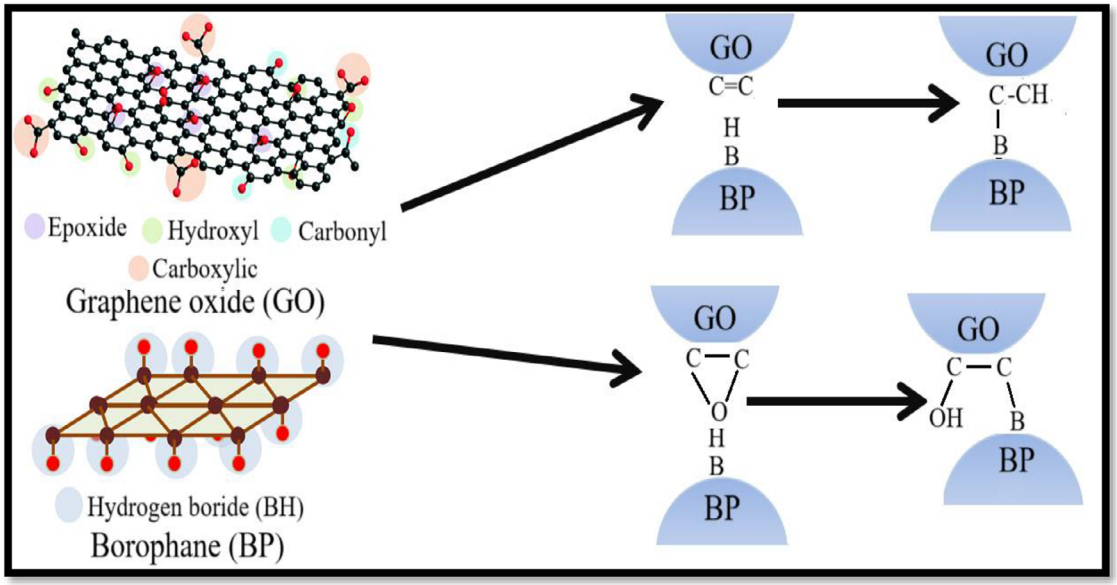

FIGURE 3 | Schematic's depicting the interaction between borophane and graphene.

(C-OH) and 287.7 (-COO groups) (Figure 4 (g)). Appearance of strong peaks at 283.9 (C-B) along with the peak corresponding to C-OH groups (~286.5 eV) confirms the ring opening reactions of epoxide and hydroboration reaction as proposed in schematic representation (Figure 3). Interestingly, the prepared composites (Figure 4 (h)) having the presence of >C = O and C-OH groups which was confirmed by data separation of O1s spectra of BG displays two peaks at 531 and 533 eV.

FE-SEM and TEM were used for the morphological characteristics of MgB_2, BP and GB composites and the results are included in Figures 5 and 6. Shown in Figure 5 (a) is the morphological features of pristine MgB_2 consisting of homogenous microstructure with randomly oriented fine crystallites having an uniaxed crystal morphology (Figure 5 (a)) [34]. De-intercalation off Mg-ion in MgB_2 by ion-exchange process resulted in the formation of foam-like morphology due to the exfoliation of borophane sheets (Figure 5 (b)). On the otherhand, borophane-graphene nanocomposites displayed the distinct morphological features of the graphene and borophane resulting in the crumpled morphological structures (Figure 5 (c)). Energy dispersive X-ray analysis (EDX) results of MgB_2, BP and GB are attached in Figure 5 (d-f). All samples exhibit three main elements such as boron, oxygen and magnesium. However, the composition of magnesium drastically drops in both BP and GB confirming the successful formation of borophane and its graphene composites. Transmission electron microscopic (TEM) results of MgB_2, BP and GB are included in Figure 6. Dark contrast coloured nearly rectangular compact crystalline structures is observed in the pristine MgB_2 crystals (Figure 6(a)). The crystalline characteristics of MgB_2 is further supported by the selected area diffraction patterns (SAED) of MgB_2 (Figure 3(a), inset). De-intercalation of Mg-ion from MgB_2 resulted in the formation of exfoliated borophane nanosheets (BP) consisting of crumpled sheet like morphologies (Figure 6 (b) with amorphous features (In accordance to the SAED patterns) (Figure 6 (b) (inset)). On the otherhand, borophane-graphene composites (BG) showed a layered morphology with highly crystalline characteristics, where the borophane sheets present within the graphene sheets as depicted in Figure 6 (c). This fact is further supported by the SAED patterns of the borophane-graphene (BG) composites (Figure 6 (c) (inset)).

Borophene derivatives are known to be chemically unstable and prone to oxidation when exposed to air and moisture. To address this concern, we examined the stability of both pristine borophane and the borophane–graphene (BG) composite over time. Pristine borophane showed clear signs of degradation, including increased B–O/B–OH signals in XPS and visible surface roughening in SEM, confirming gradual oxidation. In contrast, the BG composite exhibited minimal chemical changes, and the characteristic B–H and C–B peaks remained stable. This improved stability is attributed to graphene layers acting as a protective barrier, limiting oxygen diffusion and preventing rapid degradation. These results demonstrate that graphene incorporation significantly enhances the chemical robustness of borophane, making the composite more suitable for long-term electrochemical applications.

To realize the application potential of the synthesized borophane-graphene (BG) composites to use as an electrode material in lithium-ion (Li-ion) batteries, 2032 type lithium-ion half cells were fabricated using the prepared BG composites as the anode and lithium metal as the counter and reference electrodes. The prepared half-cells were subjected to galvanostatic charge—discharge studies in the potential scale of 0.01 ~ 2.0 V set at the current rate of 100 mA/g. For comparison purpose, MgB_2 and borophane based lithium-ion cells have also been fabricated and tested for its electrochemical performances in the selected potential range (0.01 ~ 2 V) set to the current rate of 100 mA/g. Included in Figure 7 are galvanostatic charge-discharge performances of MgB_2, BP and BG composites. Earlier report on theoretical studies of MgB_2 revealed that though it is superconducting material, the monolayers can potentially be used in lithium-ion batteries as an anode material, thanks to its excellent assumed storage capacity (~1750.9 mAh/g) and low

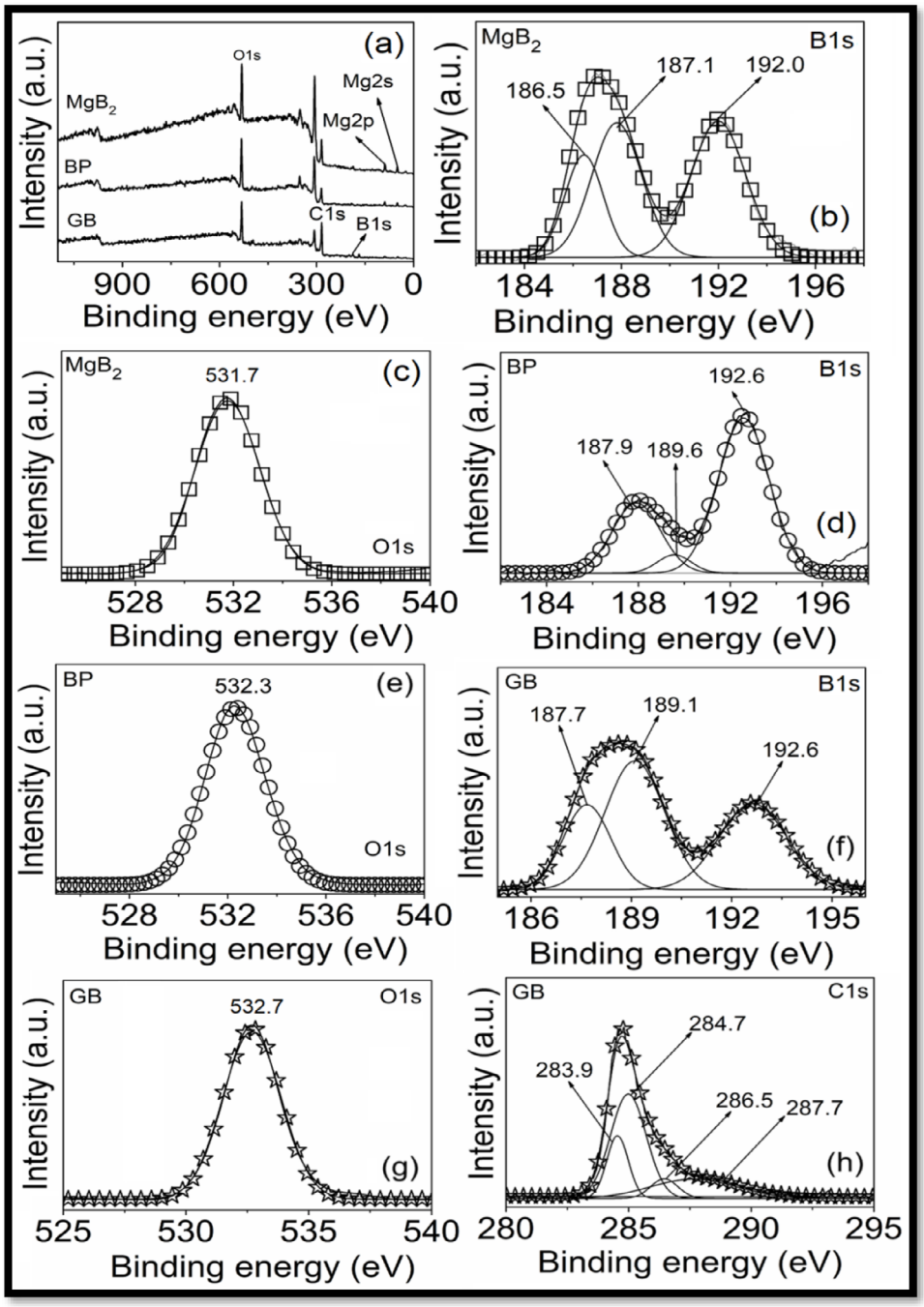

FIGURE 4 | Survey scan and high resolution XPS results of MgB_2, BP and GB composites.

open-circuit voltage values (OCV, 0.697 V) [35]. In contrast, our experimental studies indicated that MgB_2 exhibited significantly lower discharge capacity with diffused discharge pattern, consistent to the graphene based anodes. The first charge and discharge capacity of the MgB_2 anode are monitored to be 232 mAh/g and 94 mAh/g, respectively the coulombic efficiency of ~40.6 % (Figure 7 (a)). After 100 cycles, MgB_2 anode displayed stable reversible storage capacity of 80 mAh/g with the coulombic efficiency of 100 % (Figure 7 (b)). On the otherhand, our proposed borophane-graphene (BG) composites exhibited first specific discharge and charge capacity of 627 and 505 mAh/g with the capacity retention of 80.5 % (Figure 7 (c)). After 100 cycles, the charge and discharge capacities of the BG composite anode are noted to be 405 and 350 mAh/g with the coulombic efficiency of 86 % (Figure 7 (d)). To corroborate the electrochemical reactions on the electrode surfaces, the differential capacity plots (dQ/dV) of the first and 100th charge-discharge cycles have been made and the results are attached in Figure 8. The observed peaks in the dQ/dV plots corresponds to the plateaus observed in the charge/discharge curves. In case of MgB_2 based electrodes, two irreversible peaks at 0.76 V and 1.0 V, revealing the formation of solid state interface layer as well as side reactions between the electrode and the electrolyte. Absence of additional peaks in the subsequent cycles indicates the phase transitions are reversible during the electrochemical cycling. This fact is clearly supported in the dQ/dV plot (100th cycle) of MgB_2 electrodes. Similar trend

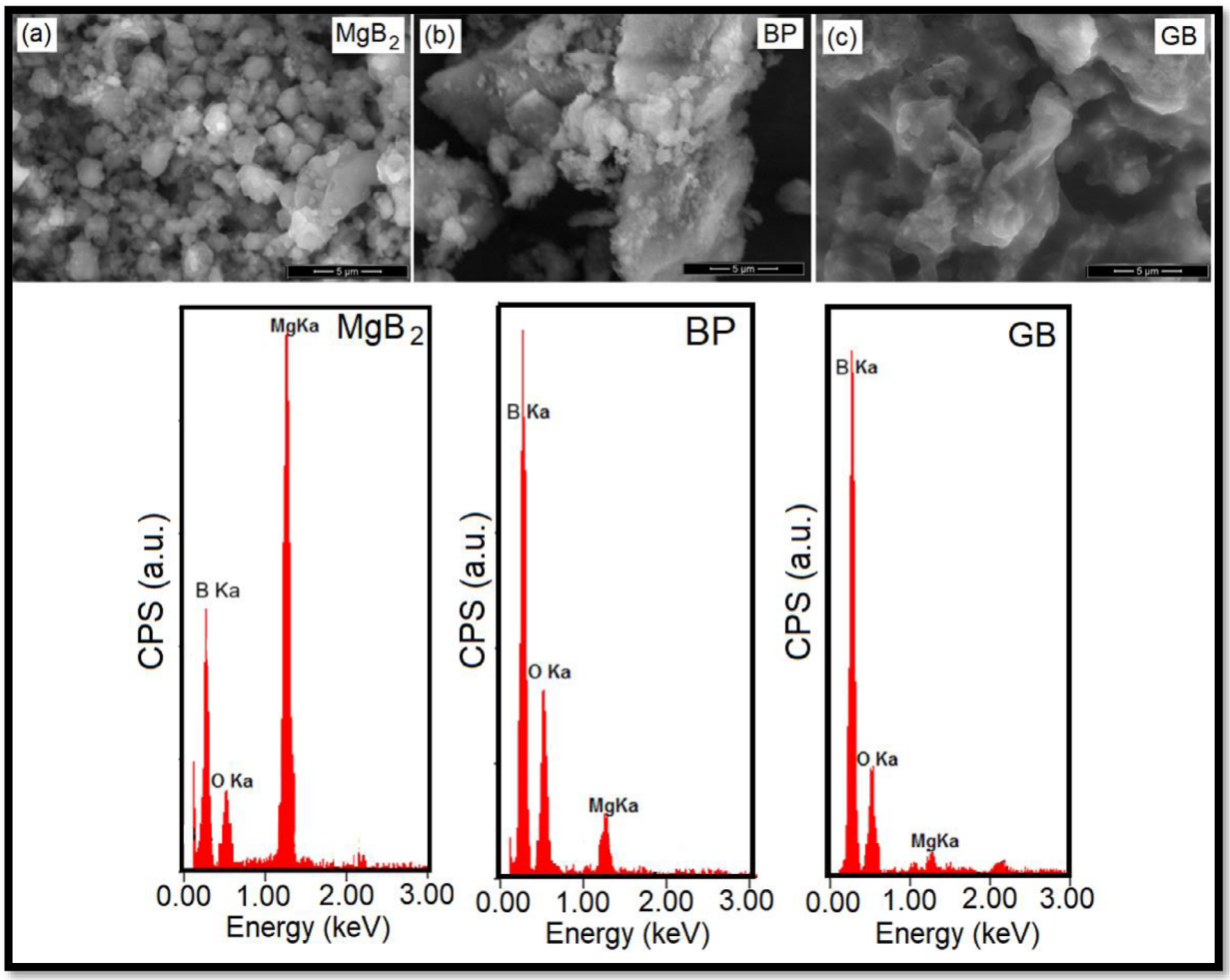

FIGURE 5 | FE-SEM and EDX results of MgB_2, BP and GB composites.

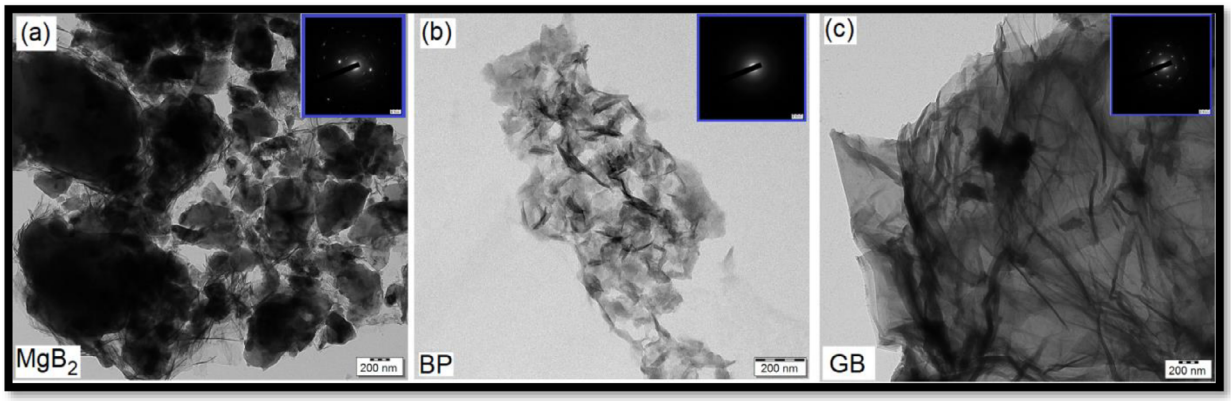

FIGURE 6 | TEM results of MgB_2, BP and GB composites.

is noted in the borophane-graphene based anodes (BG), which showed several irreversible peaks in the first discharge curve. Also, no peaks are observed in the 100th cycle of BG based electrodes quite consistent to MgB_2 based electrodes. Though, the dQ/dV results of MgB_2 and BG electrodes looks apparently same in 100th electrochemical cycling, the higher reversible storage capacity is may be attributed to the capacitance type charge storage behaviour (Electric double layer capacitance, EDLC) in the latter case.

Included in Figure 9 is the long term electrochemical cycling behaviour of MgB_2 and borophane-graphene (BG) composite electrodes. The reversible discharge storage capacity profiles for 100 repeated testing cycles measured at the current rate

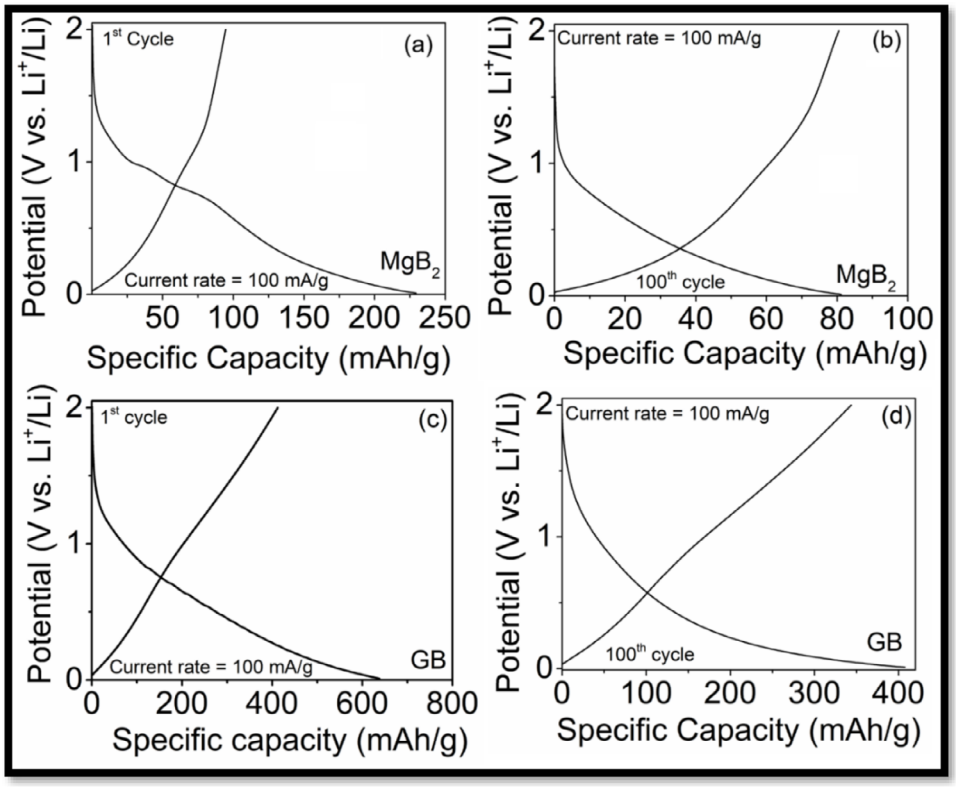

FIGURE 7 | Galvanostatic charge-discharge studies of MgB_2 (a, b) and GB composite (c, d) based anodes.

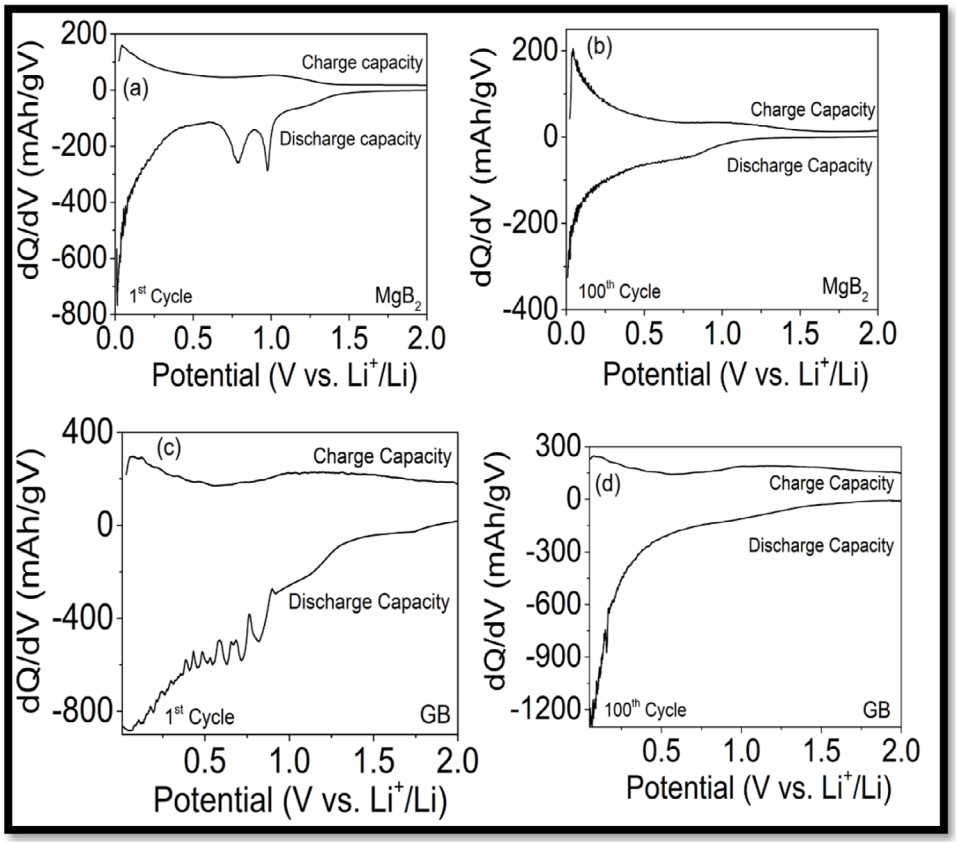

FIGURE 8 | dQ/dV vs. potential results of MgB_2 (a, b) and GB composite (c, d) based anodes.

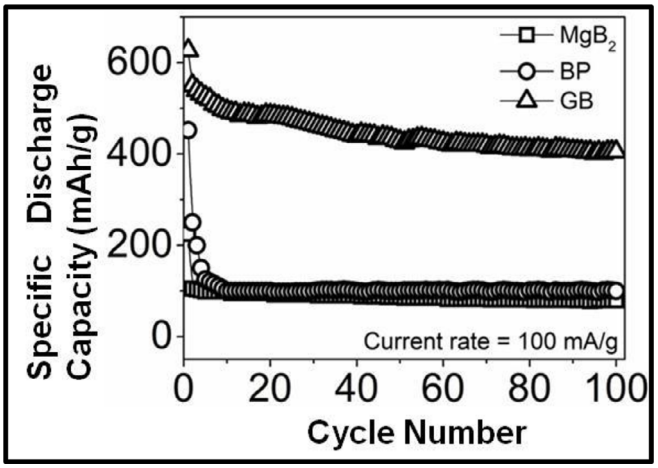

FIGURE 9 | Long term electrochemical characteristics of MgB_2, BP and GB composite anodes.

of 100 mA/g is shown in Figure 9. For comparison purpose, the extended period cycling behaviour of borophane (BP) based electrodes is also attached (Figure 9). The first discharge storage capacity of MgB_2 is observed to 232 mAh/g with significant drop in the second cycle (~90 mAh/g) with the capacity retention of only 38.8 %. After 100 cycles, MgB_2 electrodes displayed stable reversible cycling behaviour of 80 mAh/g. On the contrary, borophane nanosheet (BP) based electrodes renders first discharge capacity value of 455 mAh/g that drops to 260 mAh/g in the second cycle with the capacity retention of 57.1 %. However, steady decrement in the discharge capacity is noted upto 10 cycles, above which the specific discharge capacity values remains almost constant. The reversible capacity value of the borophane electrode after 100 cycles is 100 mAh/g and our reported results are quite consistent to the earlier experimental investigation of borophane based anode materials [36]. On the otherhand, synthesized borophane-graphene (BG) composite anode displayed first specific discharge capacity as high as 627 mAh/g with the 83.5 % retention of its initial capacity in the second cycle. However, progressive decrement in specific discharge is noted with cycle number and it renders higher reversible capacity value of ~405 mAh/g after 100 cycles corroborating enhanced electrochemical characteristics of the prepared composites. Higher reversible discharge capacity of the BG electrode is attributed to the enhanced lithium reversible adsorption sites due to the intercalation of borophane within the graphene sheets preventing the aggregation of borophane nanosheets [37–40].

A comparison table summarizing the electrochemical performance of the present work against previously reported boron-based, borophane-related, and graphene-based anode materials for Li-ion batteries (Table 1).

4 | Conclusions

In summary, a novel borophane-graphene composite anodes derived from magnesium boride (MgB_2) and natural graphite has been proposed. Structural characterization revealed the formation of composite electrodes with certain degree of crystalline characteristics. Morphological characterization corroborated the

TABLE 1 | Comparison boron-based, borophane-related, and graphene-based anode with the present borophane–Graphene (BG) composite.

Material Composition	Synthesis Method	Specific Capacity (Initial / Reversible)	Cycling Stability	Current Density	Reference
Borophene (theoretical)	First-principles DFT study	504 mAh g^{-1} (theoretical)	—	—	[14] Zhang et al., *Nanoscale*, 2016
Borophane nanosheets	Ion-exchange from MgB_2	455 / 100 mAh g^{-1}	100 cycles	100 mA g^{-1}	[41] Hou et al., *Nano Res. Energy* 2023
MgB_2 nanosheets	Chemical exfoliation	232 / 80 mAh g^{-1}	100 cycles	100 mA g^{-1}	[42] Kumar Padhi et al., Nano-Structures & Nano-Objects2023
Graphene nanosheets	Modified Hummers + reduction	350 / 300 mAh g^{-1}	100 cycles	100 mA g^{-1}	[43] Xu et al., *Chem. Rev.*, 2013
MoS_2–Graphene composite	Hydrothermal + vacuum filtration	300 / 230 mAh g^{-1}	100 cycles	100 mA g^{-1}	[8] David et al., *ACS Nano*, 2014
Graphene–siloxene composite	Interfacial chemical assembly	1200 / 1040 mAh g^{-1}	1000 cycles	500 mA g^{-1}	[7] Kumar et al., *J. Power Sources*, 2020
Phosphorene–graphene hybrid	Exfoliation + chemical reduction	1300 / 1100 mAh g^{-1}	300 cycles	100 mA g^{-1}	[44] Sun et al., *Nat. Nanotechnol.*, 2015
Borophane–Graphene composite (BG)	Ion-exchange borophane + hydroboration on GO	**627 / 405 mAh g^{-1}**	**100 cycles**	**100 mA g^{-1}**	**This Work**

formation of intercalated nanosheets in which borophane is stacked between the graphene layers. The interfacial interaction between the borophane and graphene is well supported by the chemical characterization studies. Electrochemical characterization of the borophane-graphene composite anode based lithium-ion cells rendered relatively higher specific discharge capacity (~627 mAh/g) in the first electrochemical cycling, when compared to its counterparts such as MgB_2 or borophane nanosheet (BP) based electrodes. The prepared borophane-graphene based composite electrodes displayed relatively stable cycling behaviour with the discharge capacity maximum of 405 mAh/ g after 100 repeated test cycles.

This composite developed to synergistically integrate the beneficial properties of both two-dimensional materials. Abundant active sites and high lithium-ion storage capability of Borophane and the mechanical robustness, interconnected conductive network from graphene together help to enhance the electrical chemical property than the pristine borophane or graphene. This composite design and study definitely will offer the viable pathway for developing stable, high capacity anode materials for advanced lithium-ion batteries.

Conflicts of Interest

The authors declare no conflicts of interest.

Data Availability Statement

The data that support the findings of this study are available from the corresponding author upon reasonable request.

References

1. A. K. Geim and K. S. Novoselov, "The Rise of Graphene," *Nature Materials* 6 (2007): 183–191, https://doi.org/10.1038/nmat1849.

2. M. Xu, T. Liang, M. Shi, and H. Chen, "Graphene-Like Two-Dimensional Materials," *Chemical Reviews* 113 (2013): 3766–3798, https://doi.org/10.1021/cr300263a.

3. A. K. Geim and I. V. Grigorieva, "Van der Waals Heterostructures," *Nature* 499 (2013): 419–425, https://doi.org/10.1038/nature12385.

4. K. S. Novoselov, A. Mishchenko, A. Carvalho, and A. H. Castro Neto, "2D materials and van der Waals Heterostructures," *Science* 353 (1979): 9439, https://doi.org/10.1126/science.aac9439.

5. C. R. Dean, A. F. Young, I. Meric, et al., "Boron Nitride Substrates for High-quality Graphene Electronics," *Nature Nanotechnology* 5 (2010): 722–726, https://doi.org/10.1038/nnano.2010.172.

6. H. Lim, S. I. Yoon, G. Kim, A. R. Jang, and H. S. Shin, "Stacking of Two-Dimensional Materials in Lateral and Vertical Directions," *Chemistry of Materials* 26 (2014): 4891–4903, https://doi.org/10.1021/cm502170q.

7. K. T. Kumar, M. J. Kumar Reddy, G. S. Sundari, et al., "Synthesis of Graphene-siloxene Nanosheet Based Layered Composite Materials by Tuning Its Interface Chemistry: An Efficient Anode With Overwhelming Electrochemical Performances for Lithium-ion Batteries," *Journal of Power Sources* 450 (2020): 227618, https://doi.org/10.1016/j.jpowsour.2019.227618.

8. L. David, R. Bhandavat, and G. Singh, "MoS2/graphene Composite Paper for Sodium-ion Battery Electrodes," *ACS Nano* 8 (2014): 1759–1770, https://doi.org/10.1021/nn406156b.

9. Y. Zhou, K. Maleski, B. Anasori, et al., "Ti3C2Tx MXene-Reduced Graphene Oxide Composite Electrodes for Stretchable Supercapacitors," *ACS Nano* 14 (2020): 3576–3586, https://doi.org/10.1021/acsnano.9b10066.

10. M. Sharma, A. A. Alholaisi, M. D. Alshahrani, et al., "Advances in Lithium-ion Batteries: Graphene Anodes and Lithium Iron Phosphate Cathodes," *Ionics* 31 (2025): 12523–12544, https://doi.org/10.1007/s11581-025-06798-w.

11. Y. Zhang, H. Wang, Z. Luo, et al., "An Air-Stable Densely Packed Phosphorene–Graphene Composite Toward Advanced Lithium Storage Properties," *Advanced Energy Materials* 6 (2016): 1600453, https://doi.org/10.1002/aenm.201600453.

12. X. Wu, J. Dai, Y. Zhao, Z. Zhuo, J. Yang, and X. C. Zeng, "Two-dimensional Boron Monolayer Sheets," *ACS Nano* 6 (2012): 7443–7453, https://doi.org/10.1021/nn302696v.

13. B. Feng, J. Zhang, Q. Zhong, et al., "Experimental Realization of Two-dimensional Boron Sheets," *Nature Chemistry* 8 (2016): 563–568, https://doi.org/10.1038/nchem.2491.

14. X. Zhang, J. Hu, Y. Cheng, H. Y. Yang, Y. Yao, and S. A. Yang, "Borophene as an Extremely High Capacity Electrode Material for Li-ion and Na-ion Batteries," *Nanoscale* 8 (2016): 15340–15347, https://doi.org/10.1039/C6NR04186H.

15. G. Tai, M. Xu, C. Hou, R. Liu, X. Liang, and Z. Wu, "Borophene Nanosheets as High-Efficiency Catalysts for the Hydrogen Evolution Reaction," *ACS Applied Materials & Interfaces* 13 (2021): 60987–60994, https://doi.org/10.1021/acsami.1c15953.

16. H. Liu, J. Gao, and J. Zhao, "From Boron Cluster to Two-dimensional Boron Sheet on Cu(111) Surface: Growth Mechanism and Hole Formation," *Scientific reports* 3 (2013): 1–9.

17. Y. Liu, E. S. Penev, and B. I. Yakobson, "Probing the Synthesis of Two-Dimensional Boron by First-Principles Computations," *Angewandte Chemie International Edition* 52 (2013): 3156–3159, https://doi.org/10.1002/anie.201207972.

18. A. J. Mannix, X. F. Zhou, B. Kiraly, et al., "Synthesis of Borophenes: Anisotropic, Two-dimensional Boron Polymorphs," *Science* 350, no. 1979 (2015): 1513–1516.

19. Y. Jiao, F. Ma, J. Bell, A. Bilic, and A. Du, "Two-Dimensional Boron Hydride Sheets: High Stability, Massless Dirac Fermions, and Excellent Mechanical Properties," *Angewandte Chemie* 128 (2016): 10448–10451, https://doi.org/10.1002/ange.201604369.

20. H. Nishino, T. Fujita, N. T. Cuong, et al., "Formation and Characterization of Hydrogen Boride Sheets Derived From MgB2 by Cation Exchange," *Journal of the American Chemical Society* 139 (2017): 13761–13769, https://doi.org/10.1021/jacs.7b06153.

21. N. K. Jena, R. B. Araujo, V. Shukla, and R. Ahuja, "Borophane as a Benchmate of Graphene: A Potential 2D Material for Anode of Li and Na-Ion Batteries," *ACS Applied Materials & Interfaces* 9 (2017): 16148–16158, https://doi.org/10.1021/acsami.7b01421.

22. M. Makaremi, B. Mortazavi, and C. V. Singh, "2D Hydrogenated Graphene-Like Borophene as a High Capacity Anode Material for Improved Li/Na Ion Batteries: A First Principles Study," *Materials Today Energy* 8 (2018): 22–28, https://doi.org/10.1016/j.mtener.2018.02.003.

23. X. Chen, Z. Qu, Z. Liu, and G. Ren, "Mechanism of Oxidization of Graphite to Graphene Oxide by the Hummers Method," *ACS Omega* 7 (2022): 23503–23510, https://doi.org/10.1021/acsomega.2c01963.

24. A. M. Shanmugharaj, J. H. Yoon, W. J. Yang, and S. H. Ryu, "Synthesis, Characterization, and Surface Wettability Properties of Amine Functionalized Graphene Oxide Films With Varying Amine Chain Lengths," *Journal of Colloid and Interface Science* 401 (2013): 148–154, https://doi.org/10.1016/j.jcis.2013.02.054.

25. W. S. Hummers and R. E. Offeman, "Preparation of Graphitic Oxide," *Journal of the American Chemical Society* 80 (2002): 1339, https://doi.org/10.1021/ja01539a017.

26. G. He, H. Chen, J. Zhu, F. Bei, X. Sun, and X. Wang, "Synthesis and Characterization of Graphene Paper With Controllable Properties via Chemical Reduction," *Journal of Materials Chemistry* 21 (2011): 14631–14638, https://doi.org/10.1039/c1jm12393a.

27. A. L. James and K. Jasuja, "Chelation Assisted Exfoliation of Layered Borides towards Synthesizing Boron Based Nanosheets," *RSC Advances* 7 (2017): 1905–1914, https://doi.org/10.1039/C6RA26658D.

28. S. S. Arvapalli, M. Muralidhar, and M. Murakami, "High-Performance Bulk MgB2 Superconductor Using Amorphous Nano-boron," *Journal of Superconductivity and Novel Magnetism* 32 (2019): 1891–1895.

29. A. Bateni, E. Erdem, W. Häßler, and M. Somer, "High-quality MgB2 Nanocrystals Synthesized by Using Modified Amorphous Nano-boron Powders: Study of Defect Structures and Superconductivity Properties," *AIP Advances* 9 (2019), https://doi.org/10.1063/1.5089488.

30. F. T. Johra, J. W. Lee, and W. G. Jung, "Facile and Safe Graphene Preparation on Solution Based Platform," *Journal of Industrial and Engineering Chemistry* 20 (2014): 2883–2887, https://doi.org/10.1016/j.jiec.2013.11.022.

31. E. Sadeghi, N. S. Peighambardoust, M. Khatamian, U. Unal, and U. Aydemir, "Metal Doped Layered MgB2 Nanoparticles as Novel Electrocatalysts for Water Splitting," *Scientific reports* 11 (2021): 1–13.

32. H. Yin, J. Tang, K. Yamaguchi, et al., "Adsorption of Atomic Hydrogen on Hydrogen Boride Sheets Studied by Photoelectron Spectroscopy," *Materials* 17 (2024): 4806, https://doi.org/10.3390/ma17194806.

33. A. Talapatra, S. K. Bandyopadhyay, P. Sen, P. Barat, S. Mukherjee, and M. Mukherjee, "X-ray Photoelectron Spectroscopy Studies of MgB2 for Valence state of Mg," *Physica C: Superconductivity and Its Applications* 419 (2005): 141–147.

34. S. D. Yudanto, A. Imaduddin, B. Kurniawan, and A. Manaf, "Formation of Polycrystalline MgB2 Synthesized by Powder in Sealed Tube Method With Different Initial Boron Phase," *Aip Conference Proceedings* 1945 (2018): 020027, https://doi.org/10.1063/1.5030249.

35. M. Wan, S. Zhao, Z. Zhang, and N. Zhou, "Two-Dimensional BeB2 and MgB2 as High Capacity Dirac Anodes for Li-Ion Batteries: A DFT Study," *The Journal of Physical Chemistry C* 126 (2022): 9642–9651, https://doi.org/10.1021/acs.jpcc.2c02563.

36. T. Akiyama, M. Ukai, Y. Ishii, S. Kawasaki, and Y. Hattori, "Lithium-ion Battery Electrode Properties of Hydrogen Boride," *Physical Chemistry Chemical Physics* 26 (2024): 12738–12744, https://doi.org/10.1039/D4CP00450G.

37. A. Fujino, S.-I. Ito, T. Goto, et al., "Hydrogenated Borophene Shows Catalytic Activity as Solid Acid," *ACS Omega* 4 (2019): 14100–14104, https://doi.org/10.1021/acsomega.9b02020.

38. H. Li, B. Zhang, Y. Wu, J. Hou, D. Jiang, and Q. Duan, "Hydrogenated Borophene/Blue Phosphorene: A Novel Two-dimensional Donor-acceptor Heterostructure With Shrunken Interlayer Distance as a Potential Anode Material for Li/Na Ion Batteries," *Journal of Physics and Chemistry of Solids* 155 (2021): 110108, https://doi.org/10.1016/j.jpcs.2021.110108.

39. J. Ding, H. Zheng, S. Wang, and X. Ji, "Hydrogenated Borophene Nanosheets Based Multifunctional Quasi-solid-state Electrolytes for Lithium Metal Batteries," *Journal of Colloid and Interface Science* 615 (2022): 79–86, https://doi.org/10.1016/j.jcis.2022.01.163.

40. X. Zeng, Y. Jing, S. Gao, et al., "Hydrogenated Borophene Enabled Synthesis of Multielement Intermetallic Catalysts," *Nature Communications* 14 (2023): 7414, https://doi.org/10.1038/s41467-023-43294-z.

41. C. Hou, G. Tai, Y. Liu, Z. Wu, X. Liang, and X. Liu, "Borophene-based Materials for Energy, Sensors and Information Storage Applications," *Nano Research Energy* 2 (2023): e9120051, https://doi.org/10.26599/NRE.2023.9120051.

42. S. Kumar Padhi, X. Liu, M. C. Valsania, et al., "Structure and Physicochemical Properties of MgB_2 Nanosheets Obtained via Sonochemical Liquid Phase Exfoliation," *Nano-Structures & Nano-Objects* 35 (2023): 101016, https://doi.org/10.1016/j.nanoso.2023.101016.

43. H. Xu, B. W. Zeiger, and K. S. Suslick, "Sonochemical Synthesis of Nanomaterials," *Chemical Society Reviews* 42 (2013): 2555–2567, https://doi.org/10.1039/C2CS35282F.

44. J. Sun, H. W. Lee, M. Pasta, et al., "A Phosphorene–graphene Hybrid Material as a High-capacity Anode for Sodium-ion Batteries," *Nature Nanotechnology* 10, no. 11 (2015): 980–985, https://doi.org/10.1038/nnano.2015.194.